A comparison of two dynamic subgrid closure methods for turbulent thermal convection

V. C. Wong and D. K. Lilly
Center for the Analysis and Prediction of Storms, University of Oklahoma, Norman, Oklahoma 73019-0628

(Received 20 April 1993; accepted 23 September 1993)

Two dynamic subgrid-scale (SGS) closure methods for turbulent thermal convection are described. The first method assumes the dissipation rate equals the SGS energy production rate that includes a troublesome buoyancy term, while the second method avoids this complication with a simplifying scale analysis. Tests with large-eddy simulations (LES) of thermal convection reveal that the second method is computationally efficient, and produces results agreeing with direct numerical simulation (DNS) data, as well as values predicted by the inertial subrange theory. Within the LES, the SGS representation is locally and dynamically adjusted to match the statistical structure of the smallest resolvable eddies.

I. INTRODUCTION

The closure linking the resolved scale and the unresolved SGS is critical to the successful simulation of many flows. In the widely used Smagorinsky[1] closure method, a single constant C_s is employed, and estimates of its value have been proposed analytically by Lilly,[2] and by matching with experimental data.[3] However, considerable variation of C_s has been evident in various flows, which limits the utility of a LES. Besides, the computed eddy viscosity does not vanish in laminar flow.

Recently, Germano *et al.*[4] developed a dynamic SGS model that calculates the square of C_s as a function of both space and time. Within a LES, the SGS representation will be locally and dynamically adjusted to match the statistical structure of the resolved turbulent eddies. This dynamic model has been used to compute high Reynolds number channel flows,[5] compressible flows,[6] buoyancy-driven flows,[7,8] turbulent recirculating flows,[9] stratified Ekman layer flows,[10] and flows with passive scalars.[6,7,11] Lilly[12] improved the dynamic model by applying a least squares technique for the optimization. Wong[13] proposed a dynamic closure method for the nonlinear SGS stresses.

The purpose of the present study is to determine the minimal base model needed in a dynamic SGS closure method to provide realistic results in high Reynolds number flows with scalar transport (e.g., the Rayleigh–Bénard convection). Two dynamic SGS closure methods for turbulent thermal convection are compared.

II. TWO SGS CLOSURE FORMULATIONS

A. Stratification formulation

In a LES, the time integration of the momentum, temperature, and pressure fields can be performed if the SGS stress tensor $\tau_{ij}(\equiv\overline{u_iu_j}-\bar{u}_i\bar{u}_j)$ and temperature flux $\tau_{\theta i}(\equiv\overline{\theta u_i}-\bar{\theta}\bar{u}_i)$ are known. Here, the overbar represents the spatial filtering or averaging on the grid scale (i.e., the smallest resolved scale). Large-scale variables have been recast in terms of Favre-filtered (or density-weighted) quantities. For simplicity, we do not use a special notation for Favre-filtered variables.

Upon modifying the Smagorinsky[1] model to account for buoyant effects explicitly,[14] the dynamic SGS models of Cabot[7] and Sullivan and Moeng[8] express τ_{ij} and τ_{θ_i}:

$$\tau_{ij}-\frac{\delta_{ij}}{3}\tau_{kk}=-2\nu_t\left(\bar{S}_{ij}-\frac{\delta_{ij}}{3}\bar{S}_{kk}\right), \tag{1}$$

$$\tau_{\theta_i}=-\nu_\theta\frac{\partial\bar{\theta}}{\partial x_i}, \tag{2}$$

with the eddy viscosity ν_t and eddy diffusivity ν_θ, defined as

$$\nu_t=C\bar{\Delta}^2\left(\bar{S}^2-\frac{1}{\mathrm{Pr}}\frac{g}{\theta_0}\frac{\partial\bar{\theta}}{\partial z}\right)^{1/2}, \tag{3}$$

$$\nu_\theta=\frac{C}{\mathrm{Pr}}\bar{\Delta}^2\left(\bar{S}^2-\frac{1}{\mathrm{Pr}}\frac{g}{\theta_0}\frac{\partial\bar{\theta}}{\partial z}\right)^{1/2}, \tag{4}$$

where g, θ_0, and z are the gravitational acceleration, the reference temperature and the vertical coordinate; and $\bar{S}\equiv(2\bar{S}_{ij}\bar{S}_{ij})^{1/2}$ is the measurement of the resolved strain rate tensor $\bar{S}_{ij}\equiv(\partial\bar{u}_i/\partial x_j+\partial\bar{u}_j/\partial x_i)/2$. The model coefficient C and the eddy Prandtl number Pr are assumed to be independent of the grid-filter width $\bar{\Delta}[\equiv(\Delta x_1\,\Delta x_2\,\Delta x_3)^{1/3}]$, with x_i $(i=1,2,3)$ the grid spacing in the ith direction. In (3) and (4), the buoyancy production term is generally less than, but comparable to, the strain term.[7,27]

B. Scaling formulation

Because of the buoyancy coupling in (3) and (4), an iterative scheme is needed within the stratification formulation of the dynamic modeling approach to solve for C

 1070-6631/94/6(2)/1016/8/$6.00

and Pr. Occasionally it is impossible to find a converged real solution to (3) and (4).[8] On the other hand, multiple solutions cannot generally be ruled out. In practice, the iterative scheme is terminated after ten iterations; but converged solutions can always be found a few time steps later as the flow condition changes. To circumvent these problems and generally simplify the dynamic method, we propose a new SGS closure, as outlined below.

Smagorinsky closure allows the eddy viscosity to respond to the existence and the strength of local shears, while maintaining a structure that is consistent with the existence of an inertial range surrounding the grid scale. The dynamic SGS model is based on a similar principle, but makes use of the known relationship between stresses and strain rates within a resolvable scale window to determine the model coefficients. According to Kolmogorov scaling,[15,16] the eddy viscosity ν_t can be expressed in terms of the grid-filter width $\bar{\Delta}$ and the dissipation rate ϵ by the relation

$$\nu_t = C^{2/3}\,\bar{\Delta}^{4/3}\epsilon^{1/3} \tag{5}$$

or

$$\nu_t = C_\epsilon \bar{\Delta}^{4/3}, \tag{6}$$

in which C_ϵ ($\equiv C^{2/3}\epsilon^{1/3}$) is the new model coefficient to be determined.[17] Expression (6) avoids using the assumption employed for deriving (3), that the dissipation rate ϵ equals the SGS energy production rate P, which includes a buoyancy term. Since the intermittency effect on $\epsilon^{1/3}$ is small,[18] we may assume that $\epsilon^{1/3}$, and hence C_ϵ, is insensitive to the grid-filter width. Now, by definition,

$$\nu_\theta = \frac{C_\epsilon}{\mathrm{Pr}}\,\bar{\Delta}^{4/3}. \tag{7}$$

The remaining task is to determine the model coefficients Pr and C_ϵ (or C) by utilizing the dynamic model developed by Germano *et al.*[4] and modified by Lilly.[12]

The apparent advantage in using (6) and (7) instead of (3) and (4) is the considerable reduction of computing effort by not calculating the bracket quantity in (3) and (4). In the present study, the ratio of the total computer times taken by the stratification and the scaling LES is 1.7. This advantage will be extended further in a simplification of applying the dynamic model.

III. DYNAMIC MODELING

The main premise behind dynamic SGS modeling[4] is the use of information at two different resolved scales to evaluate the model coefficients. Thereby, let us introduce a second spatial filter, with a larger filter width than the grid filter, called the "test filter." This filter generates a second set of resolvable-scale fields (denoted by $\hat{}$). In a finite differencing calculation, the test-filtered flow quantities can be obtained by volume averaging the grid-scale variables over 7 (or 27) grid cells. In this analysis, we use seven-point averaging within a test-filtering volume, with a stencil of three grid points in each direction. We also choose the test-filter scale $\hat{\Delta}=2\bar{\Delta}$, which is consistent with other three-dimensional filtering models.[7,10,19]

By direct analogy to (1), the subtest-scale (STS) stress tensor $T_{ij}(\equiv \widehat{\overline{u_i u_j}} - \hat{\bar{u}}_i \hat{\bar{u}}_j)$ is approximated by

$$T_{ij} - \frac{\delta_{ij}}{3} T_{kk} = -2\nu_T\left(\hat{\bar{S}}_{ij} - \frac{\delta_{ij}}{3}\hat{\bar{S}}_{kk}\right), \tag{8}$$

where $\hat{\bar{S}}_{ij} \equiv (\partial \hat{\bar{u}}_i/\partial x_j + \partial \hat{\bar{u}}_j/\partial x_i)/2$ and ν_T is the STS eddy viscosity (e.g., $\nu_T \approx C_\epsilon \hat{\Delta}^{4/3}$ for the scaling formulation). Similarly, the STS temperature flux $T_{\theta i}(\equiv \widehat{\overline{\theta u_i}} - \hat{\bar{\theta}}\hat{\bar{u}}_i)$ is given by

$$T_{\theta i} = -\nu_\Theta \frac{\partial \hat{\bar{\theta}}}{\partial x_i}, \tag{9}$$

where ν_Θ is the STS eddy diffusivity (e.g., $\nu_\Theta \approx C_\epsilon \hat{\Delta}^{4/3}/\mathrm{Pr}$ for the scaling formulation). The fluxes τ_{ij}, τ_{θ_i}, T_{ij}, and $T_{\theta i}$ are unknown quantities, because $\overline{u_i u_j}$, $\overline{\theta u_i}$, $\widehat{\overline{u_i u_j}}$, and $\widehat{\overline{\theta u_i}}$ contain information within the unresolved scale. However, subtracting the test-scale average of $\tau_{ij}, \tau_{\theta_i}$ from $T_{ij}, T_{\theta i}$, respectively, leads to[4]

$$L_{ij} \equiv T_{ij} - \hat{\tau}_{ij} = \widehat{\overline{u_i}\,\overline{u_j}} - \hat{\bar{u}}_i \hat{\bar{u}}_j \tag{10}$$

and

$$R_{\theta i} \equiv T_{\theta i} - \hat{\tau}_{\theta_i} = \widehat{\overline{\theta}\,\overline{u_i}} - \hat{\bar{\theta}}\hat{\bar{u}}_i. \tag{11}$$

Now, the test window elements L_{ij} and $R_{\theta i}$ are known quantities because the RHS of (10) and (11) can be directly evaluated from the resolved velocity and temperature fields. According to (1), (6), (8), and (10),

$$L_{ij} - \tfrac{1}{3}\delta_{ij} L_{kk} \approx 2C_\epsilon M_{ij}, \tag{12}$$

with $M_{ij} \equiv (\bar{\Delta}^{4/3} - \hat{\Delta}^{4/3})(\hat{\bar{S}}_{ij} - \delta_{ij}\hat{\bar{S}}_{kk}/3)$. Since $L_{ij} = L_{ji}$, (12) represents six independent equations with one unknown C_ϵ. Evidently, (12) is an overdetermined system, and it is appropriate to use a least squares method[12] to determine C_ϵ:

$$2\bar{\Delta}^{4/3} C_\epsilon \approx \frac{\langle (L_{ij} - \frac{1}{3}\delta_{ij}L_{kk})[\hat{\bar{S}}_{ij} - (\delta_{ij}/3)\hat{\bar{S}}_{kk}]\rangle}{[1-(\hat{\Delta}/\bar{\Delta})^{4/3}]\langle [\hat{\bar{S}}_{lm} - (\delta_{lm}/3)\hat{\bar{S}}_{nn}]^2\rangle}, \tag{13}$$

where $\langle\ \rangle$ indicates plane or local volume averaging.

Similarly,

$$\bar{\Delta}^{4/3}\frac{C_\epsilon}{\mathrm{Pr}} \approx \frac{\langle R_{\theta i}(\partial\hat{\bar{\theta}}/\partial x_i)\rangle}{[1-(\hat{\Delta}/\bar{\Delta})^{4/3}]\langle (\partial\hat{\bar{\theta}}/\partial x_j)^2\rangle}. \tag{14}$$

One can divide (13) by (14) to obtain the eddy Prandtl number Pr. Note that spatial averaging is required to prevent the occurrence of numerical instability.[4] In the present study, horizontal plane averaging is used to compare results from both DNS and LES.

To close the system for compressible fluid, we need to compute τ_{kk} in (1). By analogy to Yoshizawa's expression,[20] we write

$$\tau_{kk}=2C_I\bar{\Delta}^{4/3}\bar{S}. \tag{15}$$

Making use of the trace of (10) with the model of (15) for T_{kk} and τ_{kk}, we obtain

$$2\bar{\Delta}^{4/3}C_I\approx\frac{L_{kk}}{[(\hat{\Delta}/\bar{\Delta})^{4/3}-1]\langle\hat{\bar{S}}\rangle}. \tag{16}$$

According to (10), L_{kk} in (16) is non-negative, since the average of the square of a quantity is never less than the square of its average. It follows that $C_I\geqslant 0$, and thus a realizability condition (i.e., $\tau_{kk}\geqslant 0$) is satisfied.

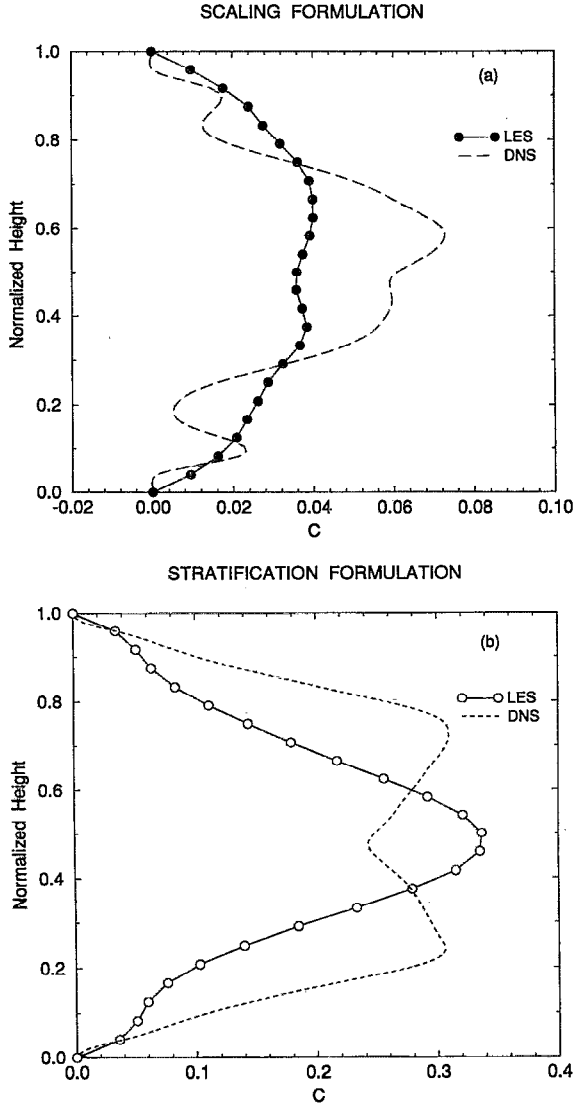

FIG. 1. Vertical profiles of the plane-averaged SGS model coefficient C. Circles represent C in LES, averaged over the third and fourth hour, and dashed lines represent C according to the DNS database. (a) C computed from scaling formulation (13), *via* (3) and (6); (b) C computed from stratification formulation (A5).

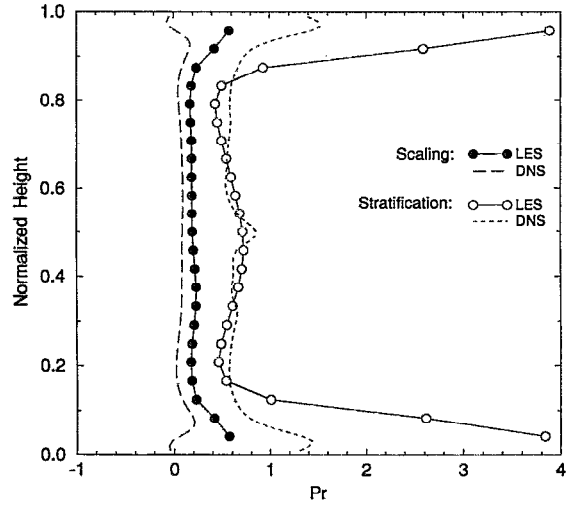

FIG. 2. Vertical profiles of the plane-averaged eddy Prandtl number Pr. Circles represent Pr in LES, averaged over the third and the fourth hour. ●: Pr computed from scaling formulation (13) and (14); ○: Pr computed from stratification formulation (A6). Dashed lines represent Pr according to the DNS database. – – –: Pr computed from scaling formulation (13) and (14); ---: Pr computed from stratification formulation (A6).

Equations (1), (2), (6), (7), and (10)–(16) form a closed SGS system, and the only input parameter for this system is the filter width ratio $\hat{\Delta}/\bar{\Delta}$. The denominator of (13) can vanish only if each component of $\hat{\bar{S}}_{ij}$ vanishes separately. In that case, the numerator also vanishes. A similar conclusion also applies to (14). At a solid boundary or for laminar flow, L_{ij} vanishes, and, according to (13)–(16), all the SGS model coefficients vanish as well. Note that Erlebacher *et al.*[21] neglected τ_{kk} on the basis that it is negligible compared to the thermodynamic pressure. In the present LES study, the ratio of the magnitudes of the gradient of τ_{kk} to the gradient of the thermodynamic pressure is indeed negligibly small.

Using (1)–(4) and (8)–(11), Sullivan and Moeng[8] calculate the coefficients C and Pr in (3) and (4) of the stratification model. Their derivation is summarized in the Appendix.

IV. RAYLEIGH–BÉNARD CONVECTION

The evaluation of the two dynamic SGS models (described in Sec. II) includes conducting *a priori tests* with a database from a DNS, and applying the SGS models to LES. The LES results are compared with DNS data and laboratory data. The flow under consideration is the turbulent Rayleigh–Bénard convection, with the bottom boundary heated and the top boundary cooled. The DNS data was taken from Moeng and Rotunno.[22] The simulation was performed with the molecular Rayleigh number $\mathrm{Ra}=3.8\times10^5$ and the molecular Prandtl number $\mathrm{Pr}'=1$. The numerical scheme is pseudospectral in the horizontal and finite difference in the vertical. The grid system consists of $96\times96\times96$ grid points for a nondimensional domain of $6\times6\times1$ for shallow convection. A sharp cutoff filter was applied as both grid and test filter to the DNS

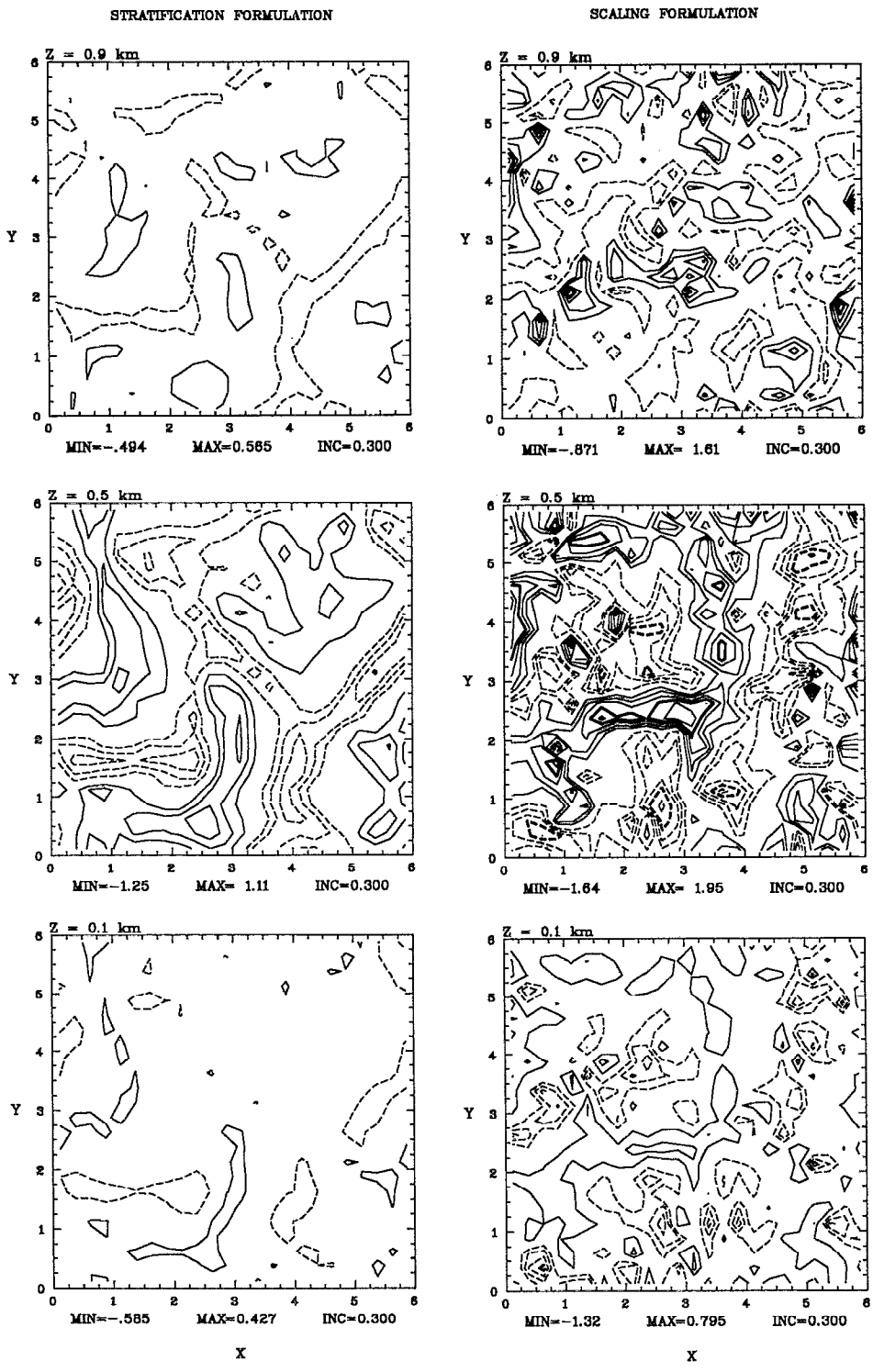

FIG. 3. Comparison of the horizontal cross sections of the LES result of w(m/s) at the fourth hour at levels z=0.1, 0.5, and 0.9 km. Solid contour lines represent $w>0$ and dashed contour lines represent $w<0$. Contour interval is 0.3 m/s.

fields to obtain the resolved velocity and temperature fields, such that the grid-scale fields are composed of modes of approximately the lowest 12 wave numbers,[8] and the test-scale filter width $\hat{\Delta}$ is equal to $2\bar{\Delta}$. Thus, the components of L_{ij} and $\hat{\bar{S}}_{ij}$ occupy the highest resolvable octave in wave space. This choice of filtering makes the resolved fields more comparable to those generated by a LES model. The resolved fields are then used to compute Pr and C_ϵ (or C)

according to (13) and (14) or (A5) and (A6). It should be noted that a DNS model also has limitations. It can only simulate low Reynolds number flow, and it has not yet resolved an inertial subrange, even on today's supercomputers.

A dry version of the Advanced Regional Prediction System (ARPS)[23] has been employed for the LES. It is a second-order staggered C-grid finite-difference compressible model in which smoothing to suppress computational noise is not invoked. A leapfrog time-difference scheme is used. The numerical resolution is $24\times24\times24$ for a domain $6\times6\times1$ km^3, with periodic lateral boundary conditions. The thermal boundary condition is constant temperature, with the temperature difference between the no-slip top and bottom boundaries equals 10 K. Vertical velocity w is zero at both boundaries. The LES was initialized with a small random perturbation of horizontal velocity and temperature at the level adjacent to the top or bottom boundary. Bulk parametrization of surface fluxes of momentum, and heat is used as lower boundary conditions for turbulent fluxes. Results generated after 4 h of time integration, corresponding to the dimensionless time $t=40$, will be discussed as follows. The time unit for Rayleigh–Bénard convection is chosen to be D/U (i.e., about 360 s), where D is the depth of the convective layer, $U\equiv(g\beta D\,\Delta\Theta)^{1/2}$, β is the coefficient of volume expansion, and $\Delta\Theta$ is the potential temperature difference between the top and bottom boundaries.

Results from the LES give the Nusselt numbers of 8.6 and 9.3 for the scaling and stratification formulations, respectively. These values are consistent with the laboratory value[24,25] of about 8 for Rayleigh number $\mathrm{Ra}\sim10^6$. Here, the Nusselt number is defined as $|\partial\theta/\partial z|\,D/\Delta\Theta$, in which the vertical gradient is evaluated at the bottom boundary.[26]

Figures 1–2 show the vertical variation of the plane-averaged values of SGS model coefficients. For comparison, the coefficient C_ϵ obtained from (13) has been converted into C, the square of the original Smagorinsky coefficient,[27] by equating (3) and (6). In Fig. 1(a), the solid circles represent the C profile computed dynamically in the LES, according to the scaling formulation (13). It approaches zero at the top and bottom boundaries, as expected, and it is consistent with the optimal values from 0.027 to 0.04 used in another LES study of the same flow,[27–30] and predicted by the inertial subrange theory.[2] It also agrees with the corresponding *a priori test* resultant C profile (long dashed line) computed from the DNS database according to (13). Figure 1(b) shows the two corresponding profiles of C, as computed according to the stratification formulation (A5). The C values are substantially larger than those obtained from the scaling formulation. The larger values of C lead to greater smoothing of the velocity fields.

In Fig. 2, the solid circles represent the vertical profile of the eddy Prandtl number Pr computed dynamically in the LES, according to the scaling formulation (13) and (14). The Pr profile is somewhat smaller than the values from 0.33 to 0.4 used in other LES studies.[27–30] However, the values of Pr, computed according to the stratification formulation, increase sharply near the top and bottom boundaries. The same feature is observed in Cabot's LES with stratification formulation.[7] It is interesting to note that the values of the Pr computed from the DNS database with the scaling formulation turn negative near the top and bottom boundaries, and the corresponding values of C and C_ϵ become slightly negative at those regions [see Fig. 1(a)],

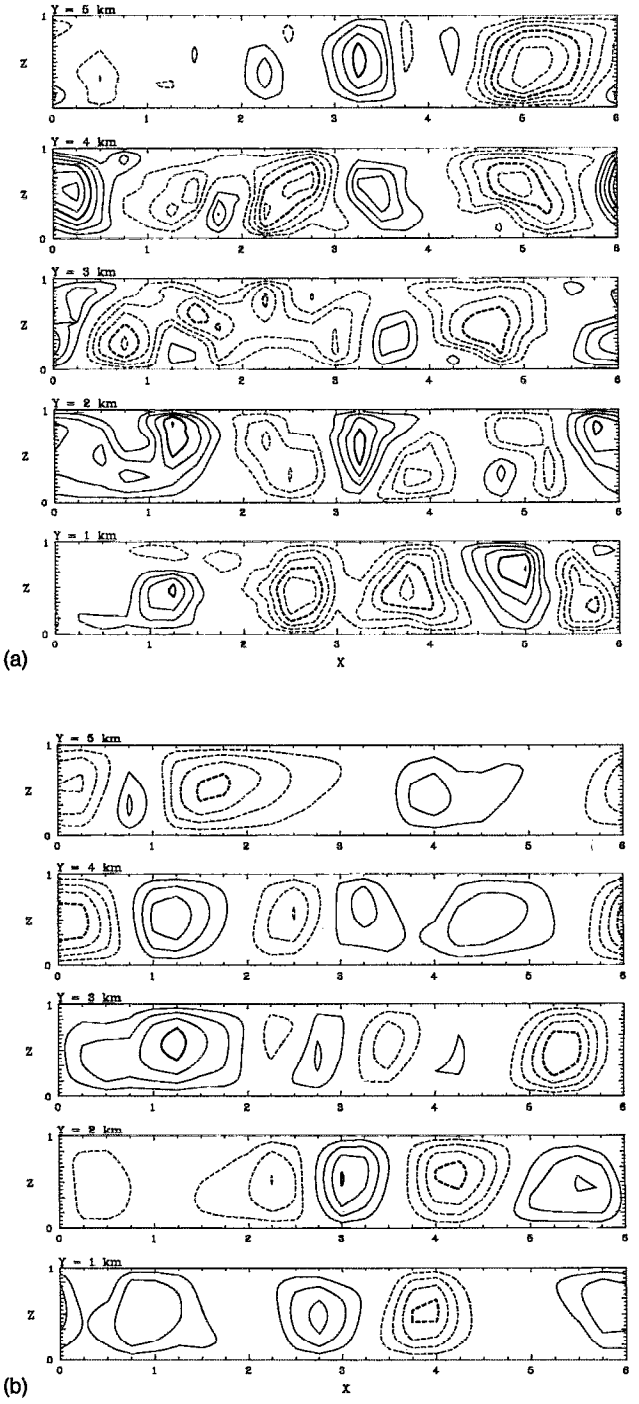

FIG. 4. Vertical cross sections of the LES result of w(m/s) at the fourth hour at meridian coordinates $y=1,2,3,4,5$ km: (a) according to the scaling formulation; (b) according to the stratification formulation. Solid contour lines represent $w>0$ and dashed contour lines represent $w<0$. Contour interval is 0.2 m/s.

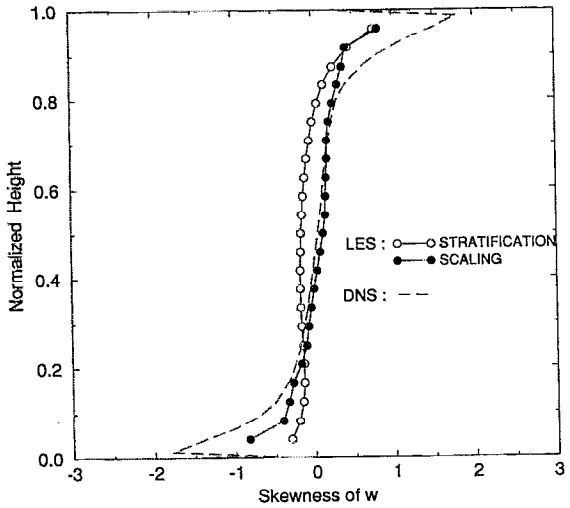

FIG. 5. Vertical profiles of the skewness of w ($\equiv \overline{w^3}/\overline{w^2}^{3/2}$). The dashed line represents DNS data.[22] Circles represent LES results at the fourth hour. ●: according to the scaling formulation; ○: according to stratification formulation.

so that the values of eddy diffusivity $\nu_\theta (\equiv C_\epsilon \bar{\Delta}^{4/3}/\mathrm{Pr})$ remain positive.

Figure 3 shows the comparison of the horizontal cross sections of the vertical velocity field w at levels $z=0.1$, 0.5, and 0.9 km, at the fourth hour of time integration. Generally, the simulated w field is weaker for the LES with stratification formulation because of the larger values of eddy viscosity.

Figures 4(a) and 4(b) show the vertical cross sections of w simulated according to the scaling and stratification formulations. In the lower layers, the area occupied by an individual updraft remains somewhat constant with height, though the vertical velocity increases with height. It indicates strong vertical circulation. Figures 4(a) and 4(b) also show that weak updrafts cannot rise to the top and that strong downdrafts produce strong low level outflows. Figure 5 shows that for the LES with the scaling formulation, the skewness of w ($\equiv \overline{w^3}/\overline{w^2}^{3/2}$) is negative in the lower layer, with a minimum value near the bottom, and positive in the upper layer, with a maximum value near the top. These results are consistent with those obtained from a DNS of Rayleigh–Bénard convection.[22] The fact that the magnitudes of the extrema for the LES are smaller than the corresponding values for the DNS is partly due to the different locations of the grid points adjacent to the top or bottom boundary. The normalized grid distance for LES and DNS are $\frac{1}{23}$ and $\frac{1}{95}$, respectively. For the LES with stratification formulation, the magnitude of the skewness of w is small in most of the domain with a maximum value near the top.

Figures 6(a) and 6(b) show that the vertical profiles of the normalized root mean squares of velocity components $\sqrt{\overline{u^2}}$ and $\sqrt{\overline{w^2}}$ simulated with the scaling formulation are closer to the DNS[22] and the laboratory[24] data than those simulated with the stratification formulation. The

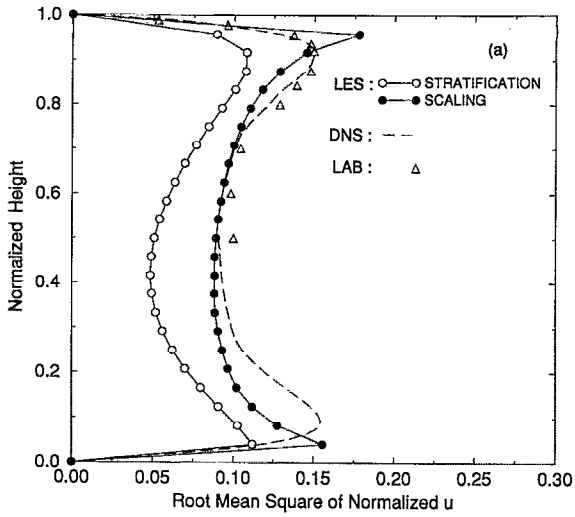

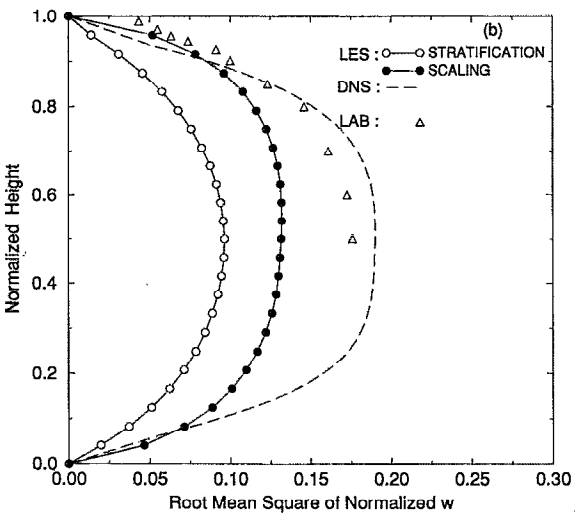

FIG. 6. Vertical profiles of the normalized root mean squares of the velocity components (a) $\sqrt{\overline{u^2}}$; (b) $\sqrt{\overline{w^2}}$. Circles represent LES results averaged over the third and the fourth hour. The dashed line represents DNS data,[22] and triangles represent laboratory data.[24]

$\sqrt{\overline{v^2}}$ profiles (not shown) are nearly identical with the $\sqrt{\overline{u^2}}$ profiles. In comparison with the DNS data near the top or bottom boundary, the larger values of $\sqrt{\overline{w^2}}$ for LES with scaling formulation contribute to smaller magnitudes of the skewness of w, as shown in Fig. 5.

V. CONCLUDING REMARKS

Two dynamic SGS closure methods for turbulent thermal convection have been compared. The stratification formulation requires an iterative scheme that is computationally inefficient. In addition, occasionally it is impossible to obtain a converged real solution for such formulation. The second method makes use of Kolmogorov scale analysis. It bypasses the aforementioned problems and the assumption that the dissipation rate ϵ equals the turbulent energy production rate P that includes a buoyancy term. It also satisfies a realizability condition for the subgrid-scale kinetic energy. This new approach works with fully developed tur-

bulence generated by shear or buoyancy. Both methods have been evaluated by performing *a priori tests* with the database from a DNS of the turbulent Rayleigh–Bénard flow, and by applying it to a LES of the same flow. The compressible model used for the LES is a staggered-grid finite-differencing model. The only input parameter for the present method is the filter width ratio $\hat{\Delta}/\bar{\Delta}$. In this study, the effect of compressibility is negligibly small, as the divergence term is negligibly small.

ACKNOWLEDGMENTS

We are grateful to C. Moeng and P. Sullivan for providing us the DNS database. Thanks are also extended to X. Song and M. Xue for programming assistance. This research was supported by the National Science Foundation through Project No. ATM-9120009. Supercomputing was provided by the Pittsburgh Supercomputing Center and the National Center for Atmospheric Research.

APPENDIX: DERIVATION OF C AND Pr

According to (1)–(4) and (8)–(11) of the stratification formulation,[8]

$$L_{ij}-\tfrac{1}{3}\delta_{ij}L_{kk}\approx 2CM_{ij}, \tag{A1}$$

$$R_{\theta i}\approx\frac{CN_{\theta i}}{\mathrm{Pr}}, \tag{A2}$$

where

$$M_{ij}\equiv\bar{\Delta}^2\overbrace{\left(\bar{S}^2-\frac{1}{\mathrm{Pr}}\frac{g}{\theta_0}\frac{\partial\bar{\theta}}{\partial z}\right)^{1/2}\bar{S}_{ij}}-\hat{\Delta}^2\left(\hat{\bar{S}}^2-\frac{1}{\mathrm{Pr}}\frac{g}{\theta_0}\frac{\partial\hat{\bar{\theta}}}{\partial z}\right)^{1/2}\hat{\bar{S}}_{ij} \tag{A3}$$

and

$$N_{\theta i}\equiv\bar{\Delta}^2\overbrace{\left(\bar{S}^2-\frac{1}{\mathrm{Pr}}\frac{g}{\theta_0}\frac{\partial\bar{\theta}}{\partial z}\right)^{1/2}\frac{\partial\bar{\theta}}{\partial x_i}}-\hat{\Delta}^2\left(\hat{\bar{S}}^2-\frac{1}{\mathrm{Pr}}\frac{g}{\theta_0}\frac{\partial\hat{\bar{\theta}}}{\partial z}\right)^{1/2}\frac{\partial\hat{\bar{\theta}}}{\partial x_i}. \tag{A4}$$

An iterative scheme is required to solve for C and Pr from (A1)–(A4). To assure a converged solution, Sullivan and Moeng[8] take the square of both (A1) and (A2) to obtain

$$C\approx\left(\frac{\langle(L_{ij}-\frac{1}{3}\delta_{ij}L_{kk})^2\rangle}{\langle(2M_{ij})^2\rangle}\right)^{1/2} \tag{A5}$$

and

$$\mathrm{Pr}\approx\left(\frac{\langle N_{\theta i}^2\rangle\langle(L_{ij}-\frac{1}{3}\delta_{ij}L_{kk})^2\rangle}{\langle R_{\theta i}^2\rangle\langle(2M_{ij})^2\rangle}\right)^{1/2}. \tag{A6}$$

At each level, iteration by successive substitution is employed to solve for C and Pr, since both M_{ij} and $N_{\theta i}$ on the RHS of (A5) and (A6) contain Pr. Again, τ_{kk} in (1) is negligibly small in the present LES study of thermal convection.

[1] J. Smagorinsky, "General circulation experiments with the primitive equations," Mon. Weather Rev. **91**, 99 (1963).
[2] D. K. Lilly, "The representation of small-scale turbulence in numerical simulation experiments," in Proceedings of the IBM Scientific Computational Symposium on Environmental Science, 1967, p. 195.
[3] J. W. Deardorff, "On the magnitude of the subgrid-scale eddy coefficient," J. Comput. Phys. **7**, 120 (1971).
[4] M. Germano, U. Piomelli, P. Moin, and W. H. Cabot, "A dynamic subgrid-scale eddy viscosity model," Phys. Fluids A **3**, 1760 (1991).
[5] U. Piomelli, "High Reynolds number calculations using the dynamic subgrid-scale stress model," Phys. Fluids A **5**, 1484 (1993).
[6] P. Moin, K. Squires, W. Cabot, and S. Lee, "A dynamic subgrid-scale model for compressible turbulence and scalar transport," Phys. Fluids A **3**, 2746 (1991).
[7] W. Cabot, "Large eddy simulations of time-dependent and buoyancy-driven channel flows," in *CTR Annual Research Briefs 1992* (Center for Turbulence Research, Stanford University/NASA Ames, 1992), p. 45.
[8] P. Sullivan and C.-H. Moeng. "An evaluation of the dynamic subgrid scale model in buoyancy driven flows," in Proceedings of the 10th Symposium on Turbulence and Diffusion, Portland, Oregon, 1992, p. 82.
[9] Y. Zang, R. L. Street, and J. R. Koseff, "A dynamic mixed subgrid-scale model and its application to turbulent recirculating flows," Phys. Fluids A **5**, 3186 (1993).
[10] M. Bohnert and J. H. Ferziger, "The dynamic subgrid scale model in large-eddy simulation of the stratified Ekman layer," in Proceedings of the 2nd International Symposium on Engineering Turbulence Modelling and Measurements, Florence, Italy, 1993.
[11] W. Cabot and P. Moin, "Large eddy simulation of scalar transport with the dynamic subgrid-scale model," in *Large Eddy Simulation of Complex Engineering and Geophysical Flows*, edited by B. Galperin and S. A. Orszag (Cambridge U.P., Cambridge, 1992).
[12] D. K. Lilly, "A proposed modification of the Germano subgrid scale closure method," Phys. Fluids A **4**, 633 (1992).
[13] V. C. Wong, "A proposed statistical-dynamic closure method for the linear or nonlinear subgrid-scale stresses," Phys. Fluids A **4**, 1080 (1992).
[14] D. K. Lilly, "On the numerical simulation of buoyant convection," Tellus **15**, 148 (1962).
[15] L. F. Richardson, "Atmospheric diffusion shown on a distance neighbor graph," Proc. R. Soc. London, Ser. A **110**, 709 (1926).
[16] A. N. Kolmogorov, "The local structure of turbulence in incompressible viscous fluid for very large Reynolds numbers," Dokl. Akad. Nauk SSSR **30**, 301 (1941).
[17] K. R. Sreenivasan, "On the scaling of the turbulence energy dissipation rate," Phys. Fluids **27**, 1048 (1984).
[18] V. R. Kuznetsov, A. A. Praskovsky, and V. A. Sabelnikov, "Fine-scale turbulence structure of intermittent shear flows," J. Fluid Mech. **243**, 595 (1992).
[19] S. Ghosal, T. S. Lund, and P. Moin, "A local dynamic model for LES," in *CTR Annual Research Briefs 1992* (Center for Turbulence Research, Stanford University/NASA Ames, 1992), p. 3.
[20] A. Yoshizawa, "Statistical theory for compressible turbulence shear flows, with the application to subgrid modeling," Phys. Fluids **29**, 2152 (1986).
[21] G. Erlebacher, M. Y. Hussaini, C. G. Speziale, and T. A. Zang, "Toward the large-eddy simulation of compressible turbulent flows," J. Fluid Mech. **238**, 155 (1992).
[22] C.-H. Moeng and R. Rotunno, "Vertical-velocity skewness in buoyancy-driven boundary layer," J. Atmos. Sci. **47**, 1149 (1990).
[23] *Advanced Regional Prediction System User's Guide*, Center for the Analysis and Prediction of Storms, University of Oklahoma, 1992, p. 183.
[24] J. W. Deardorff and G. E. Willis, "Investigation of turbulent thermal convection between horizontal plates," J. Fluid Mech. **28**, 675 (1967).
[25] D. C. Threlfall, "Free convection in low-temperature gaseous helium," J. Fluid Mech. **28**, 675 (1967).
[26] W. Cabot, "Large eddy simulations of passive and buoyant scalars with dynamic subgrid-scale models," in *CTR Annual Research Briefs 1991* (Center for Turbulence Research, Stanford University/NASA Ames, 1991), p. 191.

[27]T. M. Eidson, "Numerical simulation of turbulent Rayleigh-Bénard convection using subgrid scale modeling," J. Fluid Mech. **158**, 245 (1985).
[28]C.-H. Moeng, "A large-eddy simulation for the study of planetary boundary layer turbulence," J. Atmos. Sci. **41**, 2052 (1984).
[29]J. W. Deardorff, "Three dimensional numerical study of turbulence in an entraining mixed layer," Boundary Layer Meteorol. **7**, 199 (1974).
[30]H. Schmidt and U. Schumann, "Coherent structure of the convective boundary layer derived from large-eddy simulations," J. Fluid Mech. **200**, 511 (1989).